An analytical study of electronic properties of ABC-stacking multilayer graphene

Cheng-Peng Chang *

Center for General Education, Tainan University of Technology, Tainan 710, Taiwan

arXiv:1704.06875v1 [cond-mat.mes-hall] 23 Apr 2017

Abstract

We present an analytical model to study the electronic properties, including full band structure, low energy dispersions around the Dirac point and density of states of the ABC-stacking N-layer graphene (ABCNLG). An ABCNLG can be simulated by a linear atomic chain with $2N$ atoms. With only nearest-neighbor inter- and intra-layer hopping integrals taken into account, the Hamiltonian representation is a complex $2N \times 2N$ tridiagonal matrix H_0. Through a unitary transformation, we can reduce the $2N \times 2N$ Hamiltonian matrix into two real $N \times N$ tridiagonal matrices $\mathbb{H}_s$ and $\mathbb{H}_a$, i. e., $H_0 = \mathbb{H}_s \oplus \mathbb{H}_a$. What's more, the two matrices satisfy the relation $\mathbb{H}_a = -\mathbb{H}_s$. As a result, energy spectrum associated with $\mathbb{H}_s$ and $\mathbb{H}_s$ have the relation $\lambda_a = -\lambda_s$. Such a characteristic is reflected on the energy dispersions and density of states. Our model can be applied to explore the basic properties of linear chain model and the eigenvalue problem of the tridiagonal matrices.

[0]Corresponding author. Tel/Fax: +886-62-545329

E-mail address: t00252@mail.tut.edu.tw (C. P. Chang)

1 Introduction

Graphene, a pristine two-dimensional (2D) material, is isolated by the exfoliation method [1], and it also offers a display place to exhibit fundamental properties of 2D system. Due to the specular geometry structure, graphene shows many interesting electronic properties, e. g., low-lying linear energy bands, electron-hole symmetry, high room-temperature mobility, high in-plane thermal conductivity Klein tunneling, and anomalous quantum Hall effect [2–9]. Multilayer graphene, one of the carbon allotropes, is the pile of several graphene layers, bound together by the van der Waals interactions, along the stacking direction. The low-energy electronic structures are strongly related to the stacking types and the number of layers [9–23]. The usually studied stacking sequences of graphene multilayers are the Bernal-stacking (AB-stacking), simple hexagonal stacking (AA-stacking), and rhombohedral stacking (ABC-stacking). Bernal-stacking (AB-stacking) bilayer graphene has attracted intense interest because its bandgap can be controlled by applying to an external electric field [10, 20–23]. With the controllable bandgap, Bernal-stacking bilayer graphene shows great potential as a new material for opto-electronic devices. In the absence of the external field, Bernal bilayer graphene is semimetal because of the tiny touch between valence and conduction bands. Two groups of the parabolic band around the Dirac points are presented in Bernal bilayer graphene [10, 20]. The electronic properties of AB-stacking multilayer graphenes also inspire a large number of studies owing to possible applications. Study results exhibit that the AB-stacking N-layer graphenes with even N layers (with odd N layers) are to be equivalent to the superposition of $N/2$ bilayer graphenes ($\frac{N-1}{2}$ bilayer graphene and one graphene-like monolayer) [15, 21].

Before the experimental realization of the AA-stacking graphite, the AA-stacking bilayer graphene, due to its simple geometrical structure, is usually utilized as a theoretical model to demonstrate the low-energy electronic properties, two pairs of nearly linear bands, which are distinguishable from those of the AB-stacking bilayer graphene because of the different stacking types. Recently, the fabrication of AA-stacking graphite [24] and the AA-stacking multilayer graphenes [25] renew interest in the fundamental properties of AA-stacking bilayer and multilayer graphenes, e.g. infrared and Raman spectra, Landau-level energies, transport, plasma excitations, magneto-absorption spectra and dynamical conductivity [26–33]. The study results exhibit that the electronic properties of the AA-stacking N-layer graphene can be treated as the superposition of N independent graphene-like monolayers [32, 33].

The electronic properties of an ABCNLG, e. g. , the flat band, bulk band, bulk band gap, electron velocity, and density-of-state, are strongly dependent on stacking order and modified by the application of a vertical electric field [34–39]. They are clearly distinct from those of AA- or AB-stacking multilayer graphenes. Most studies focus on the low-energy electronic structures of ABC-stacking trilayer graphene. A non-perturbative effective Hamiltonian closed in the bulk subspace is proposed to explore the bulk subbands for arbitrary the layer number N [39]. Recently, experimental approval of the extended flat bands and the gapped subbands in ABC-stacking multilayer graphene has been reported [40,41]. The above-mentioned experimental works trigger us to revisit the electronic properties of ABCNLG. We present an analytical model to effectively and efficiently study full band structure, low energy dispersions around the Dirac point and density of states.

2 Theory and Model

The geometrical structure of an ABCNLG is shown in Fig. 1(a). Each graphene layer is a one-atom-thickness layer, in which carbon atoms are precisely packed in a hexagonal lattice. The lattice contains two sublattices A and B, represented by white and black circles, respectively. A primitive cell contains two atoms and the nearest carbon-carbon distance is $b = 1.42$Å. Within ABCNLG, half of the atoms are directly below atoms in the adjacent sheet and directly above hexagonal ring centers and the other half of the atoms are directly above atoms and directly below hexagonal ring centers [42]. A primitive cell of an ABCNLG has $2N$ carbon atoms, denoted as, $A_1, B_1, A_2, B_2, \cdots, A_l, B_l, \cdots, A_N, B_N$. The first Brillouin zone is also shown in Fig. 1(a). The atom-atom interactions, shown in Fig. 1(a), are as follows. β_0 represents the interaction between atom A and B on the same graphene layer. The interlayer interaction between the atom A and B from the two neighboring layers is β_1 while the two atoms have the same (x, y) coordinate. The distance between the two nearest neighboring sheets is $c = 3.35$ Å. The values of β_0 and β_1 are [42] $\beta_0 = 3.16$ eV and $\beta_1 = 0.36$ eV.

The Hamiltonian representation H_0, expanded in the set of 2D Bloch functions, ($|A_1\rangle$,

$|B_1\rangle$, $|A_2\rangle$, $|B_2\rangle$, $\cdots\cdots$, $|A_{N-1}\rangle$,$|B_{N-1}\rangle$, $|A_N\rangle$,$|B_N\rangle$), is a $2N \times 2N$ matrix and reads

$$H_0 = \begin{pmatrix}
0 & \beta_0\mathbf{f_k} & 0 & 0 & 0 & \cdots & \cdots & 0 & 0 & 0 & 0 & 0 \\
\beta_0\mathbf{f_k^*} & 0 & \beta_1 & 0 & 0 & \cdots & \cdots & 0 & 0 & 0 & 0 & 0 \\
0 & \beta_1 & 0 & \beta_0\mathbf{f_k} & 0 & \cdots & \cdots & 0 & 0 & 0 & 0 & 0 \\
0 & 0 & \beta_0\mathbf{f_k^*} & 0 & \beta_1 & \cdots & \cdots & 0 & 0 & 0 & 0 & 0 \\
0 & 0 & 0 & \beta_1 & \ddots & \ddots & \cdots & 0 & 0 & 0 & 0 & 0 \\
\vdots & \vdots & \vdots & \vdots & \ddots & \ddots & \ddots & 0 & \vdots & \vdots & \vdots & \vdots \\
\vdots & \vdots & \vdots & \vdots & 0 & \ddots & \ddots & \ddots & \vdots & \vdots & \vdots & \vdots \\
0 & 0 & 0 & 0 & 0 & \cdots & \ddots & 0 & \beta_1 & 0 & 0 & 0 \\
0 & 0 & 0 & 0 & 0 & \cdots & \cdots & \beta_1 & 0 & \beta_0\mathbf{f_k} & 0 & 0 \\
0 & 0 & 0 & 0 & 0 & \cdots & \cdots & 0 & \beta_0\mathbf{f_k^*} & 0 & \beta_1 & 0 \\
0 & 0 & 0 & 0 & 0 & \cdots & \cdots & 0 & 0 & \beta_1 & 0 & \beta_0\mathbf{f_k} \\
0 & 0 & 0 & 0 & 0 & \cdots & \cdots & 0 & 0 & 0 & \beta_0\mathbf{f_k^*} & 0
\end{pmatrix}_{2N\times 2N}, \quad (1)$$

where $\mathbf{f_k} = \sum_{j=1}^{3} \exp(i\mathbf{k}\cdot\mathbf{b}_j) = fe^{i\theta}$ and $\theta = tan^{-1}(\frac{Im[\ \mathbf{f_k}\ ]}{Re[\ \mathbf{f_k}\ ]})$; $\mathbf{b}_j$ represents the three nearest neighbors on the same graphene plane and $\mathbf{k}$ is the in-plane wave vector. Obviously, H_0 is a tridiagonal matrix with complex elements resulting from the complex structure factor $\mathbf{f_k}$. It is more efficient to diagonalize a real matrix for eigenvalues than a complex one. Such a complex tridiagonal matrix (Eq. (1)) can be easily transformed into a real symmetrical matrix through a unitary transformation. By adopting the new 2D Bloch functions ($\phi_1 = |A_1\rangle,\ \phi_2 = e^{i\theta}|B_1\rangle,\ \phi_3 = e^{i\theta}|A_2\rangle,\ \phi_4 = e^{i2\theta}|B_2\rangle,\ \cdots\cdots, \phi_{2N-3} = e^{i(N-2)\theta}|A_{N-2}\rangle,\ \phi_{2N-2} = e^{i(N-1)\theta}|B_{N-l}\rangle,\ \phi_{2N-1} = e^{i(N-1)\theta}|A_N\rangle,\ \phi_{2N} = e^{iN\theta}|B_N\rangle$), we calculate the Hamiltonian matrix element $\mathcal{H}(i,j) = \langle\phi_i|H_0|\phi_j\rangle$ and the transferred Hamiltonian representation is

obtained as follows

$$\mathcal{H}=\begin{pmatrix}
0 & \beta_0 f & 0 & 0 & 0 & \cdots & \cdots & 0 & 0 & 0 & 0 & 0 \\
\beta_0 f & 0 & \beta_1 & 0 & 0 & \cdots & \cdots & 0 & 0 & 0 & 0 & 0 \\
0 & \beta_1 & 0 & \beta_0 f & 0 & \cdots & \cdots & 0 & 0 & 0 & 0 & 0 \\
0 & 0 & \beta_0 f & 0 & \beta_1 & \cdots & \cdots & 0 & 0 & 0 & 0 & 0 \\
0 & 0 & 0 & \beta_1 & \ddots & \ddots & \cdots & 0 & 0 & 0 & 0 & 0 \\
\vdots & \vdots & \vdots & \vdots & \ddots & \ddots & \ddots & 0 & \vdots & \vdots & \vdots & \vdots \\
\vdots & \vdots & \vdots & \vdots & 0 & \ddots & \ddots & \ddots & \vdots & \vdots & \vdots & \vdots \\
0 & 0 & 0 & 0 & 0 & \cdots & \ddots & 0 & \beta_1 & 0 & 0 & 0 \\
0 & 0 & 0 & 0 & 0 & \cdots & \cdots & \beta_1 & 0 & \beta_0 f & 0 & 0 \\
0 & 0 & 0 & 0 & 0 & \cdots & \cdots & 0 & \beta_0 f & 0 & \beta_1 & 0 \\
0 & 0 & 0 & 0 & 0 & \cdots & \cdots & 0 & 0 & \beta_1 & 0 & \beta_0 f \\
0 & 0 & 0 & 0 & 0 & \cdots & \cdots & 0 & 0 & 0 & \beta_0 f & 0
\end{pmatrix}_{2N\times 2N}. \tag{2}$$

The Hamiltonian matrix of an ABCNLG is now transformed into a real and symmetrical matrix.

According to Eq. (2), an ABCNLG can be modeled as a linear atomic chain of carbon atoms, as shown in Figs. (1b) and (1c). In order to reduce the dimension of Hamiltonian matrix, we further construct the symmetrized basis functions: $|\psi_1^s, \psi_2^s, \cdots, \psi_i^s, \cdots, \psi_{N-1}^s, \psi_N^s, \psi_1^a, \psi_2^a, \cdots, \psi_i^a, \cdots, \psi_{N-1}^a, \psi_N^a\rangle$. Based on the mirror symmetry, or inversion symmetry, of linear atomic chain, they are divided into two groups, symmetrical and anti-symmetrical groups, and organized as follows:

$$\begin{cases}
\psi_1^s = (\phi_1 + \phi_{2N})/\sqrt{2} \\
\vdots \\
\psi_j^s = (\phi_j + \phi_{2N+1-j})/\sqrt{2} \\
\vdots \\
\psi_N^s = (\phi_N + \phi_{N+1})/\sqrt{2} \\
\psi_1^a = (\phi_1 - \phi_{2N})/\sqrt{2} \\
\vdots \\
\psi_j^a = (\phi_j - \phi_{2N+1-j})/\sqrt{2} \\
\vdots \\
\psi_N^a = (\phi_N - \phi_{N+1})/\sqrt{2}
\end{cases}$$

After some manipulation, the $2N \times 2N$ Hamiltonian matrix H_0 is decomposed into two $N \times N$ diagonal-block matrices, i. e., the reduced Hamiltonian matrix reads

$$\mathbb{H}_{red} = \begin{pmatrix} \mathbb{H}_s & 0 \\ 0 & \mathbb{H}_a \end{pmatrix}. \tag{3}$$

It is noted that the two diagonal-block matrices satisfy the relation $\mathbb{H}_s(i,j) = -\mathbb{H}_a(i,j)$. This is to say, the reduced Hamiltonian representation has the characteristics, $\mathbb{H}_{red} = \mathbb{H}_s \oplus \mathbb{H}_a$ and $\mathbb{H}_s = -\mathbb{H}_a$.

The representation actually $\mathbb{H}_s$ depends on the layer number N. When $N = 2m + 1$ is odd, the representation of the block matrix $\mathbb{H}_s$ is

$$\mathbb{H}_s = \begin{pmatrix} 0 & \beta_0 f & 0 & 0 & 0 & \cdots & \cdots & 0 & 0 \\ \beta_0 f & 0 & \beta_1 & 0 & 0 & \cdots & \cdots & 0 & 0 \\ 0 & \beta_1 & 0 & \beta_0 f & 0 & \cdots & \cdots & 0 & 0 \\ 0 & 0 & \beta_0 f & 0 & \beta_1 & \cdots & \cdots & 0 & 0 \\ 0 & 0 & 0 & \beta_1 & \ddots & \ddots & \cdots & 0 & 0 \\ \vdots & \vdots & \vdots & \vdots & \ddots & \ddots & \ddots & \vdots & \vdots \\ \vdots & \vdots & \vdots & \vdots & \ddots & \ddots & \ddots & \beta_0 f & \vdots \\ 0 & 0 & 0 & 0 & \cdots & \ddots & \beta_0 f & 0 & \beta_1 \\ 0 & 0 & 0 & 0 & 0 & \cdots & \cdots & \beta_1 & \beta_0 f \end{pmatrix}_{N \times N}. \tag{4}$$

$\mathbb{H}_s$ is a real tridiagonal matrix with a non-zero element occurring at the corner $\mathbb{H}_s(N,N) = \beta_0 f$. As is shown in Fig. 1(b), the ABC-stacking trilayer graphene is described by an atomic chain with $2N = 6$ atoms. The decomposition of $\mathcal{H}$ (Eq.(2)) into $\mathbb{H}_s$ and $\mathbb{H}_a$ (Eq.(3)) is equivalent to cutting a long atomic chain into two short atomic chains and each chain is made up of $N = 3$ atoms. One surface atom of the short chain has the site-energy $\beta_0 f$ (or $-\beta_0 f$). On the other hand,

$$\mathbb{H}_s = \begin{pmatrix} 0 & \beta_0 f & 0 & 0 & 0 & \cdots & \cdots & 0 \\ \beta_0 f & 0 & \beta_1 & 0 & 0 & \cdots & \cdots & 0 \\ 0 & \beta_1 & 0 & \beta_0 f & 0 & \cdots & \cdots & 0 \\ 0 & 0 & \beta_0 f & 0 & \beta_1 & \cdots & \cdots & 0 \\ 0 & 0 & 0 & \beta_1 & \ddots & \ddots & \cdots & 0 \\ \vdots & \vdots & \vdots & \vdots & \ddots & \ddots & \ddots & \vdots \\ \vdots & \vdots & \vdots & \vdots & \ddots & \ddots & \ddots & \beta_0 f \\ 0 & 0 & 0 & 0 & \cdots & \ddots & \beta_0 f & \beta_1 \end{pmatrix}_{N \times N}, \tag{5}$$

when the layer number $N(=2m)$ is even. For instance, the ABC-stacking quad-layer graphene is simulated by an 8-atom chain, as is shown in Fig. 1(c). The reduced Hamiltonian matrix $\mathbb{H}_s$ ($\mathbb{H}_a$) is modeled by a 4-atom chain (the right panel of Fig. 1(c). Each 4-atom chain has two asymmetrical surface atoms. The renormalized surface atom has site-energy β_1 ($-\beta_1$).

The eigen-equation of ABCNLG ($H_0|\mathbf{u}_0\rangle = \lambda|\mathbf{u}_0\rangle$) is now decomposed into two eigen-equations, which are

$$\mathbb{H}_\xi|\boldsymbol{u}_\xi\rangle = \lambda_\xi|\boldsymbol{u}_\xi\rangle, \tag{6}$$

where $\xi = s$ or a denotes the symmetrical or anti-symmetrical state. The eigenenergy spectrum $\lambda_a = -\lambda_s$ because of $\mathbb{H}_a = -\mathbb{H}_s$. Moreover, $\mathbb{H}_a$ and $\mathbb{H}_s$ share the same eigenvector $|\boldsymbol{u}_\xi\rangle$, i. e., $|\boldsymbol{u}_s\rangle = |\boldsymbol{u}_a\rangle$. Once the eigenenergy spectrum λ_s of $\mathbb{H}_s$ is acquired, the eigenenergy spectrum λ_a is thus obtained through the relation $\lambda_a = -\lambda_s$.

3 Energy spectra of ABCNLGs

3.1 Energy spectrum of $N = 3$ ABCNLG

The reduction of the size of Hamiltonian matrix allows us easily and efficiently to acquire the eigenenergies of ABCNLG. The analytical form of eigenenergy of $N = 3$ ABCNLG is obtained by solving the secular equation $|\mathbb{H}_s - \lambda\mathbb{I}| = 0$, where $\mathbb{I}$ is the identity matrix and λ is eigenvalues. The secular equation associated with the trilayer graphene is

$$|\mathbb{H}_s - \lambda\mathbb{I}| = det\begin{vmatrix} -\lambda & \beta_0 f & 0 \\ \beta_0 f & -\lambda & \beta_1 \\ 0 & \beta_1 & \beta_0 f - \lambda \end{vmatrix}_{3\times 3} = 0. \tag{7}$$

The secular equation is a cubic polynomial $\lambda^3 + r\lambda^2 + s\lambda + t = 0$, where the coefficients are $r = -\beta_0 f$, $s = -(\beta_0^2 f^2 + \beta_1^2)$ and $t = \beta_0^3 f^3$. The roots of secular equation are the eigenenergy spectrum $\lambda_j^{(N)}$ ($j = 1, 2, 3$). The close form of $\lambda_j^{(3)}$ is

$$\begin{cases} \lambda_1^{(3)} = -r/3 + \left[P - \sqrt{Q^3 + P^2}\right]^{1/3} + \left[P + \sqrt{Q^3 + P^2}\right]^{1/3}, \\ \lambda_2^{(3)} = -r/3 + e^{\pi/3}[P - \sqrt{Q^3 + P^2}]^{1/3} - e^{-\pi/3}[P + \sqrt{Q^3 + P^2}]^{1/3}, \\ \lambda_2^{(3)} = -r/3 + e^{-\pi/3}[P - \sqrt{Q^3 + P^2}]^{1/3} - e^{\pi/3}[P + \sqrt{Q^3 + P^2}]^{1/3}, \end{cases} \tag{8}$$

where $P = \dfrac{-r^3}{27} + \dfrac{st}{6} - \dfrac{t}{2}$ and $Q = \dfrac{s}{3} - \dfrac{r^2}{9}$.

3.2 Energy spectrum of $N = 4$ ABCNLG

The secular equation realted to ABCNLG with $N = 4$ is

$$|\mathbb{H}_s - \lambda\mathbb{I}| = det \begin{vmatrix} -\lambda & \beta_0 f & 0 & 0 \\ \beta_0 f & -\lambda & \beta_1 & 0 \\ 0 & \beta_1 & -\lambda & \beta_0 f \\ 0 & 0 & \beta_0 f & \beta_1 - \lambda \end{vmatrix}_{4\times 4} = 0. \tag{9}$$

It is a fourth order polynomial $\lambda^4 - \beta_1\lambda^3 - (\beta_1^2 + 2\beta_0^2 f^2)\lambda^2 + \beta_1(\beta_1^2 + \beta_0^2 f^2)\lambda + \beta_0^4 f^4 = 0$. The roots $\lambda_j^{(4)}$ of the secular equation are the energy spectrum.

3.3 The calculated energy spectrum

Energy spectrum of ABC-stacking N-layer graphene can be acquired by the exact diagonalization using numerical l ibrary or by solving the roots of the associated secular equation. First, the energy dispersions of ABC-stacking trilayer graphene, as is shown in Fig. 2(a), are used to check the correction of our model. The red curves are the energy dispersions of the symmetrical Hamiltonian $\mathbb{H}_s$. They are the eigenvalues obtained by the numerical diagonalization method. We further apply the relation $\lambda_a = -\lambda_s$ to gain the energy dispersions of the asymmetrical Hamiltonian $\mathbb{H}_a$, the green curves. The dashed curves are calculated by employing Eq.(8), the close form of the eigenenergy. The dashed curves are completely identical to the red curves.

As is shown in Fig. 2(b), the energy dispersions of ABC-stacking quad-layer ($N = 4$) graphene are obtained by the diagonalization of matrices, H_0, $\mathcal{H}$ and $\mathbb{H}_s$ (Eq. (1), Eq.(2) and Eq.(3)). The entire overlap of three sets of energy dispersions exhibits that the reduced Hamiltonian matrix $\mathbb{H}_s$ can efficiently offer the eigenenergy spectrum.

An ABCNLG illustrates N branches of the energy dispersion. Each branch is closely similar to the energy dispersions of a monolayer graphene, such as the maximum of the energy dispersion occurring at the point Γ, the discontinuity presented near the saddle point M and the nearly linear bands appearing around the K point.

3.4 Low-energy spectrum around the Dirac point

Our model can clearly reveal the characteristic of the low-energy electronic structures. Figures 3(a)-3(h) present the low-energy bands of ABCNLG with the layer number N. There are N red (green) curves, which are the energy dispersions of Hamiltonian $\mathbb{H}_s$ ($\mathbb{H}_a$). The red curves are symmetrical to the green ones about the Fermi energy $E_F = 0$. The

electronic structures of an ABCNLG show linear bands, flat bands and Mexican-hat bands. The flat bands, existing near the E_F, originate in the surface state. The extension of the flat bands increases with the increase of the number of layers. The remainder bands are the $2N-2$ bulk bands. The highest conduction bands and the lowest valence bands are nearly linear bands. An AA-stacking N-layer graphene presents N pairs of linear bands. An AB-stacking multilayer graphene illustrates parabolic bands and linear bands.

The low-energy bands of an ABCNLG also depend on whether the layer number N is odd or even. The red curves shows one surface state, $\frac{N-1}{2}$ conduction bands and $\frac{N-1}{2}$ valence bulk bands when $N=2m+1$ is odd. At the Dirac point $\mathbf{K}$, $f_{\mathbf{k}}=0$ and the eigenvalue of $\mathbb{H}_s$ are $\lambda_j=0,\ \pm\beta_1,\ \pm\beta_1,\cdots,\pm\beta_1$. On the other hand, there are one surface state, $\frac{N}{2}$ conduction bands and $\frac{N}{2}-1$ valence bulk bands when $N=2m$ is even. At the Dirac point $\mathbf{K}$, the eigenvalue of $\mathbb{H}_s$ is $\lambda_j=0,\beta_1,\pm\beta_1,\pm\beta_1,\cdots,\pm\beta_1$.

The properties of the flat bands are investigated. The flat bands is closely located at $\lambda\sim 0$. By setting $\lambda\sim 0$ in the secular equation and neglecting the high order terms of λ, the secular equation related to ABC-stacking trilayer graphene is $-(\beta_0^2f^2+\beta_1^2)\lambda+\beta_0^3f^3=0$ and, thus, the eigenenergy of the flat band is obtained $\lambda=\frac{\beta_0^3f^3}{\beta_0^2f^2+\beta_1^2}\approx\frac{\beta_0^3f^3}{\beta_1^2}$ because of $\beta_0 f\ll\beta_1$ in the vicinity of the point $\mathbf{K}$. The secular equation of ABC-stacking quad-layer graphene is approximated as $\beta_1(\beta_1^2+\beta_0^2f^2)\lambda+\beta_0^4f^4=0$ and the eigenenergy of the flat band reads $\lambda=-\frac{\beta_0^4f^4}{\beta_1(\beta_1^2+\beta_0^2f^2)}\approx-\frac{\beta_0^4f^4}{\beta_1^3}$.

The wave function associated with the flat band of an ABCNLG is calculated. The eigenenergy of the flat band of ABC-stacking trilayer graphene is $\lambda=\frac{\beta_0^3f^3}{\beta_1^2}$. After inserting λ into eigen equation (Eq.(6)), we acquire the eigen equation as follows

$$\begin{bmatrix} 0 & \beta_0 f & 0 \\ \beta_0 f & 0 & \beta_1 \\ 0 & \beta_1 & \beta_0 \end{bmatrix}\begin{bmatrix} u_1 \\ u_2 \\ u_3 \end{bmatrix}=\frac{\beta_0^3f^3}{\beta_1^2}\begin{bmatrix} u_1 \\ u_2 \\ u_3 \end{bmatrix}. \tag{10}$$

The transverse of the eigen state $|\boldsymbol{u}_\xi\rangle^T$ is $(u_1,u_2,u_3)=(1,\frac{\beta_0^2f^2}{\beta_1^2},\frac{\beta_0^5f^5}{\beta_1^5}-\frac{\beta_0 f}{\beta_1})\sim(1,0,0)$ because of $\beta_0 f\sim 0$. The wave function is $\Psi=u_1\psi_1^s+u_2\psi_2^s+u_3\psi_3^s=(\phi_1+\phi_{2N})/\sqrt{2}$. The electrons are localized at outermost layers of the ABCNLG with $N=3$. The eigen state $(u_1,u_2,u_3,u_4)^T$ of the ABC-stacking quad-layer graphene is gained by solving the

eigen-equation

$$\begin{bmatrix} 0 & \beta_0 f & 0 & 0 \\ \beta_0 f & 0 & \beta_1 & 0 \\ 0 & \beta_1 & 0 & \beta_0 f \\ 0 & 0 & \beta_0 f & \beta_1 \end{bmatrix} \begin{bmatrix} u_1 \\ u_2 \\ u_3 \\ u_4 \end{bmatrix} = \lambda \begin{bmatrix} u_1 \\ u_2 \\ u_3 \\ u_4 \end{bmatrix}. \tag{11}$$

The eigen state $|\boldsymbol{u}_\xi\rangle^T$ is $(u_1, u_2, u_3, u_4) = (1, (\frac{\beta_0 f}{\beta_1})^3, (\frac{\beta_0 f}{\beta_1})^7 - \frac{\beta_0 f}{\beta_1}, -(\frac{\beta_0 f}{\beta_1})^{10} + (\frac{\beta_0 f}{\beta_1})^4 + (\frac{\beta_0 f}{\beta_1})^2) \sim (1, 0, 0, 0)$. The wave function is $\Psi = u_1\psi_1^s + u_2\psi_2^s + u_3\psi_3^s + u_4\psi_4^s = (\phi_1 + \phi_{2N})/\sqrt{2}$, i. e., the electrons are presented in the outermost layers.

4 Density of state of an ABCNLG

Density of state (DOS), which reveals the main features of the electronic structures, is defined as

$$D(\omega) = \frac{2}{\pi} \sum_{j=1}^{j=2N} \int_{1stBZ} \frac{d^2\mathbf{k}}{(2\pi)^2} \frac{\Gamma}{(\lambda_j(\mathbf{k_x}, \mathbf{k_y}) - \omega)^2 - \Gamma^2}. \tag{12}$$

Γ (=0.001 β_0) is the phenomenological broadening parameter. The summation Σ runs over all the subband index j, starting at $j = 1$ and ending at $j = 2N$. The $2N$ subbands are divided into two groups, symmetrical and asymmetrical groups. The summation is rearranged as $\sum_{j=1}^{2N} = \sum_{j_s=1}^{N} + \sum_{j_a=1}^{N}$ and DOS $D(\omega)$ is decomposed into two parts $D_s(\omega)$ and $D_a(\omega)$. That is:

$$D(\omega) = D_s(\omega) + D_a(\omega), \tag{13}$$

where $D_s(\omega) = -D_a(\omega)$ because of $\lambda_s = -\lambda_a$.

DOS of $N = 3$, 4, 5, and 6 ABCNLGs are presented by the black curves in Figs. 4(a)-4(d). The low energy DOS of $N = 3$, 4, 5, and 6 ABCNLGs are exhibited in Fig. 5. The special features in the DOS, including sharp peak, square-root divergences, logarithmic singularity, and discontinuity are immediately associated with the structures of the energy dispersions [Figs. 2 and 3]. The flat bands, as is shown in Fig. 3, give rise to a sharp peak located at $E_F = 0$ [Fig. 5]. Energy bands near $\pm\beta_1$ ($\pm$0.36 eV), are presented as concave-upward (concave-downward) parabolic bands, leading to square-root divergences. DOS has N logarithmic peaks near $\omega \sim \pm\beta_0$ (3.16 eV) [insets in the right panel of figure 4], resulting from the separated saddle points near the M point in Fig. 2. The maximum (or minimum) of the energy dispersions occurring at the point Γ [Fig. 2] brings about the discontinuity at $\omega \sim \pm 3\beta_0$.

The red (green) curves in Figs 4 and 5 are DOS $D_s(\omega)$ ($D_a(\omega)$) related to the energy bands of symmetrical (asymmetrical) group, the eigenenergy of Hamiltonian $\mathbb{H}_s$ ($\mathbb{H}_a$). The calculated results illustrate that $D_s(\omega) \neq D_s(-\omega)$ and $D_a(\omega) \neq D_a(-\omega)$, and the sub-DOS $D_s(\omega)$ ($D_a(\omega)$) is not symmetry about $E_F = 0$. The red curves are symmetrical to the green ones about $E_F = 0$, i. e., $D_s(\omega) = D_a(-\omega)$. The low energy DOS, presented in Fig. 5, exhibits that whether the layer number N is odd or even has a great effect on the detail structures of DOS.

5 CONCLUSIONS

The electronic properties of the ABC-stacking N-layer graphenes are explored through the tight-binding method, based on the minimal model, including only the main inter- and intra-layer interactions. An ABCNLG can be modeled as a linear atomic chain with $2N$ atoms and described by a complex $2N \times 2N$ tridiagonal matrix H_0, which is further reduced into two real $N \times N$ tridiagonal matrices $\mathbb{H}_s$ and $\mathbb{H}_a$, i. e., $H_0 = \mathbb{H}_s \oplus \mathbb{H}_a$ through a unitary transformation. Most importantly, the two matrices are shown to have the relation $\mathbb{H}_a = -\mathbb{H}_s$. The eigenenergies of $\mathbb{H}_s$ and those of $\mathbb{H}_s$ have the relation $\lambda_a = -\lambda_s$. The transformation of a complex $2N \times 2N$ tridiagonal matrix H_0 into a real $N \times N$ tridiagonal matrix allows us to efficiently explore the full band structure, low energy dispersions and DOS. Above all, our analytical model can be utilized to study the eigenvalue problem of linear chain model and the tridiagonal Toeplitz matrix.

Acknowledgement

The authors gratefully acknowledge the support of the Ministry of Science and Technology of Taiwan, under Grants No. MOST105-2112-M-165-001-MY3.

References

[1] Novoselov KS, Geim AK, Morozov SV, Jiang D, Zhang Y, Dubonos SV, et al. Electric field effect in atomically thin carbon films. Science 2004; 306(5696):666-9.

[2] Novoselov KS, Geim AK, Morozov SV, Jiang D, Katsnelson MI, Grigorieva IV, et al. Two-dimensional gas of massless Dirac Fermions in graphene. Nature 2005;438(10):197-200.

[3] Zhang YB, Tan YW, Stormer HL, Kim P. Experimental observation of the quantum Hall effect and Berry's phase in graphene. Nature 2005; 438(10):201-4.

[4] Gusynin VP, Sharapov SG. Unconventional integer quantum Hall effect in graphene. Phys Rev Lett 2005; 95(14):146801.

[5] McCann E, Fal'ko VI. Landau-level degeneracy and quantum hall effect in a graphite bilayer. Phys Rev Lett 2006; 96(8):086805.

[6] Peres NMR. The transport properties of graphene: An introduction. Rev Mod Phys 2100; 82(3):2673-2700.

[7] Abergela DSL, Apalkovb V, Berashevicha J, Zieglerc K, Chakrabortya T. Properties of graphene: a theoretical perspective. Adv Phys 2010; 59(4):261-482.

[8] Basov DN, Fogler MM , Lanzara A, Wang F, Zhang Y . Colloquium: Graphene spectroscopy. Rev Mod Phys 2014; 86:959.

[9] Castro Neto AH, Guinea F, Peres NMR, Novoselov KS, Geim AK. The electronic properties of graphene. Rev Mod Phys 2009; 81(1):109-62.

[10] Latil S, Henrard L. Charge carriers in few-layer graphene films. Phys Rev Lett 2006; 97(3):036803.

[11] Lu CL, Chang CP, Huang YC, Chen RB, Lin MF. The influence of electric field on optical properties of the few-layer graphene with AB-stacking. Phys Rev. B 2006; 73(14):144427.

[12] Lu CL , Chang CP, Huang YC, Ho JH, Hwang CC , Lin MF. Electronic Properties of AA- and ABC-Stacked Few-Layer Graphites, Journal of the Physical Society of Japan 2007; 76 : 024701.

[13] Graf D, Molitor F, Ensslin K, Stampfer C, Jungen A, Hierold C, et al. Spatially resolved raman spectroscopy of single- and few-layer graphene. Nano Lett 2007; 7(2):238-42.

[14] Nilsson J, Castro Neto AH, Guinea F, Peres NMR. Electronic properties of bilayer and multilayer graphene. Phy Rev B 2008; 78(4):045405.

[15] M Koshino, T Ando. Magneto-optical properties of multilayer graphene. Phy Rev B 2008; 77 (11): 115313.

[16] Reina A, Jia XT, Ho J, Nezich D, Son H, Bulovic V, et al. Large area few-layer graphene films on arbitrary substrates by chemical vapor deposition. Nano Lett 2009; 9(1):30-5.

[17] Avetisyan AA, Partoens B, Peeters FM. Stacking order dependent electric field tuning of the band gap in graphene multilayers. Phys Rev B 2012; 81(11):115432.

[18] Craciun MF, Russo S, Yamamoto M, Oostinga JB, Morpurgo AF, Tarucha S. Trilayer graphene is a semimetal with a gate-tunable band overlap. Nat Nanotech 2009; 4(6):383-8.

[19] Lui CH, Li Z, Mak KF, Cappelluti E, Heinz TF. Observation of an electrically tunable band gap in trilayer graphene. Nat Phys 2010; 7(12):944-7.

[20] Chang CP. Analytic model of energy spectrum and absorption spectra of bilayer graphene. J Appl Phys 2012; 111(10):103714.

[21] Chang CP. Energy dispersions and minimal conductivity of bernal multilayer graphene. J Phys Chem C 2012; 116(41):22073-7.

[22] McCann E, Koshino M. The electronic properties of bilayer graphene. Reports on Progress in Physics. 2013; 76(5): 056503.

[23] Rozhkova AV, Sboychakova AO, Rakhmanova AL, Franco Noria. Electronic properties of graphene-based bilayer systems. Physics Reports 2016; 648: 1-104

[24] Lee JK, Lee SC, Ahn JP, Kim SC, Wilson JIB, John P. The growth of AA graphite on (111) diamond. J Chem Phys 2008; 129(23): 234709.

[25] Borysiuk J, Soltys J, Piechota J. Stacking sequence dependence of graphene layers on SiC (000-1)- Experimental and theoretical investigation. J Appl Phys 2011; 109(9):093523.

[26] Liu Z, Suenaga K, Harris PJF, Iijima S. Open and closed edges of graphene layers. Phys Rev Lett 2009; 102(1):015501.

[27] Xu YH, Li XW, Dong JM. Infrared and Raman spectra of AA-stacking bilayer graphene. Nanotechnology 2010; 21(6):065711.

[28] Ho YH, Wu JY, Chen RB, Chiu YH, Lin MF. Optical transitions between Landau levels: AA-stacked bilayer graphene. Appl Phys Lett 2010; 97(10):101905.

[29] Chang CP. Exact solution of the spectrum and magneto-optics of multilayer hexagonal graphene. J Appl Phys 2011; 110(1):013725.

[30] Tabert CJ, Nicol EJ. Dynamical conductivity of AA-stacked bilayer graphene. Phys Rev B 2012; 86(7):075439.

[31] Lin MF, Chuang YC, Wu JY. Electrically tunable plasma excitations in AA-stacked multilayer graphene. Phys Rev B 2012; 86(12):125434.

[32] Chang CP. Exact Landau spectrum and wave functions of biased AA-stacked multilayer graphene. Carbon 2013; 61:209-215.

[33] Chang CP. Dynamical conductivity of gated AA-stacking multilayer graphene with spin-orbital coupling. RSC Adv 2015; 5:32511-32519.

[34] Koshino M. Interlayer screening effect in graphene multilayers with ABA and ABC stacking. Phy Rev B 2010, 81(12):125304.

[35] Zhang F, Sahu B, Min H, MacDonald AH. Band structure of ABC-stacked graphene trilayers. Phy Rev B 2010, 82(3):035409.

[36] Yuan S, Roldan R, Katsnelson MI. Landau level spectrum of ABA- and ABC-stacked trilayer graphene. Phys Rev B 2011; 84:125455.

[37] Koshino M. Stacking-dependent optical absorption in multilayer graphene. New Journal of Physics 2013; 15:015010.

[38] Yi-Ping Lin, Chiun-Yan Lin, Cheng-Pong Chang and Min-Fa Lin. Electric-field-induced rich magneto-absorption spectra of ABC-stacked trilayer graphene. RSC Adv 2015; 5:80410-80414.

[39] Ching-Hong Ho, Cheng-Peng Chang, and Ming-Fa Lin. Evolution and dimensional crossover from the bulk subbands in ABC-stacked graphene to a three-dimensional Dirac cone structure in rhombohedral graphite. Phy Rev B 2016; 93:075437.

[40] Henni Y, Collado HPO, Nogajewski K, Molas MR, Usaj G, Balseiro CA, et al.. Rhombohedral multilayer graphene: A magneto-Raman scattering study. Nano Lett 2016; 16(6):3710-3716.

[41] Bao C, Yao W, Wang E, Chen C, Avila J, Asensio MC , Zhou Shu. Stacking-Dependent Electronic Structure of Trilayer Graphene Resolved by Nanospot Angle-Resolved Photoemission Spectroscopy. Nano Lett 2017 ;17(3): 1564-1568.

[42] Charlier JC, Michenaud JP, Lambin P. Tight-binding density of electronic states of pregraphitic carbon. Phys Rev B 1992; 46(8):4540-3.

Figure Captions

FIG. 1. (a) exhibits the geometric structure, the intralayer interaction, and the interlayer interaction of ABC-stacking trilayer graphene. The hexagonal ring is the first Brillouin zone. (b) The ABC-stacking trilayer graphene is modeled by a six-atom chain. Along the chain, the nearest neighbor interactions $\beta_0 f$ and β_1 are labeled. The six-atom chain is cut into two 3-atom chains. The site energy of the surface atom, marked by red circle, is $\beta_0 f$ (or $-\beta_0 f$). (c) The same plot as (b) but for the ABC-stacking quad-layer graphene.

FIG. 2. (a) The full energy band of the ABC-stacking trilayer graphene. (b) The same plot as (a) but for the ABC-stacking quad-layer graphene.

FIG. 3. (a)-(c) present the low energy dispersions of the ABC-stacking multilayer graphenes with layer numbers $N = 3$, 5, and 7. The low energy dispersions of the ABC-stacking multilayer graphenes $N = 4$, 6, and 8 are shown in (d)-(f). The red (green) curve illustrates the energy spectrum of the reduced Hamiltonian matrix $\mathbb{H}_s$ ($\mathbb{H}_a$).

FIG. 4. DOS of the ABC-stacking multilayer graphenes with layer numbers $N = 3$, 4, 5, and 6. The red (green) curve is DOS related to $D_s(\omega)$ ($D_a(\omega)$).

FIG. 5. (a)-(d) present the low energy DOS of ABC-stacking multilayer graphenes with layer numbers $N = 3$, 5, 7 and 15. The low energy DOS of ABC-stacking multilayer graphenes $N = 4$, 6, 8 and 16 are shown in (e)-(h). The sub-DOS $D_s(\omega)$ ($D_a(\omega)$) is marked by the red (green) curve .

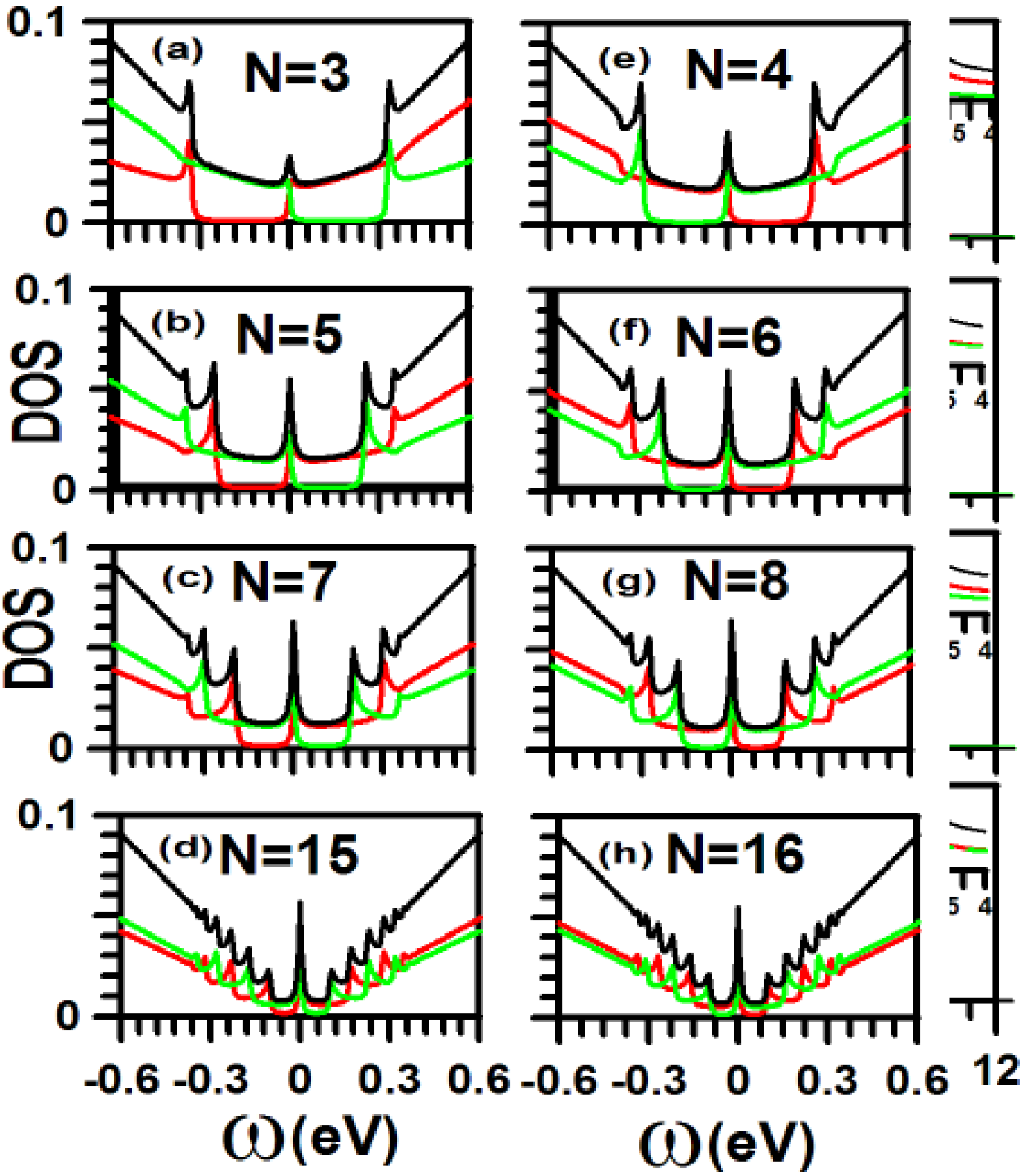

FIG. 5